

RSC Advances



This is an *Accepted Manuscript*, which has been through the Royal Society of Chemistry peer review process and has been accepted for publication.

Accepted Manuscripts are published online shortly after acceptance, before technical editing, formatting and proof reading. Using this free service, authors can make their results available to the community, in citable form, before we publish the edited article. This *Accepted Manuscript* will be replaced by the edited, formatted and paginated article as soon as this is available.

You can find more information about *Accepted Manuscripts* in the [Information for Authors](#).

Please note that technical editing may introduce minor changes to the text and/or graphics, which may alter content. The journal's standard [Terms & Conditions](#) and the [Ethical guidelines](#) still apply. In no event shall the Royal Society of Chemistry be held responsible for any errors or omissions in this *Accepted Manuscript* or any consequences arising from the use of any information it contains.

High dielectric permittivity and low loss tangent of polystyrene incorporated with hydrophobic core-shell copper nanowires

Linxiang He, Sie Chin Tjong*

Department of Physics and Materials Science, City University of Hong Kong, Hong Kong

Email: aptjong@um.cityu.edu.hk Tel.: (852) 34427702 Fax: (852) 34420538

ABSTRACT: We reported a low-cost strategy to improve dielectric performance of polystyrene (PS) by incorporating core-shell copper nanowires (CuNWs). The hydrothermally synthesized nanowires had a fresh copper core coated with a hydrophobic insulating layer. Compared with pure PS, CuNW/PS nanocomposites exhibited drastically improved dielectric performance, as manifested by their large dielectric permittivity (ϵ') and low loss tangent ($\tan\delta$). At 16 wt.% CuNWs loading, dielectric permittivity of the composite reaches 37 at 1 MHz, which was about 14 times larger than that of neat PS ($\epsilon' = 2.5$). While the loss tangent of this composite was maintained at a low level ($\tan\delta = 0.04$). The pronounced dielectric improvement was ascribed to a large electrical conductivity of the fresh core of CuNWs, which provided the composites with a higher amount of mobile charge carriers participating in the interfacial polarization. The low loss tangent was attributed to the presence of insulating layer on the CuNWs, which impaired the formation of an electrically conductive network, thus suppressing dielectric loss. This simple strategy may open a new avenue to increasing dielectric permittivity of polymers while maintaining relatively low loss tangent.

Keywords: Copper nanowires; Polymer composite; Dielectric permittivity; Loss tangent;

1. Introduction

Polymer nanocomposites with a high dielectric permittivity (high- k) have great potential to store electrical energy and therefore can be used for a broad range of functional applications, such as communication devices, actuators, charge-storage capacitors, etc. [1-4]. Easy processability of the polymer matrix draws a promising future for these materials [5-7]. However, low dielectric permittivity of the polymer matrix still poses a challenge for obtaining high- k polymer composites. Conventional process typically used to increase the dielectric permittivity is by incorporating high- k insulating ceramic fillers into the polymer matrix to form a composite [8-15]. To meet the demanding requirements for practical applications, however, a large amount of ceramic fillers is usually required, resulting in a loss of flexibility of the resultant material. Another strategy is to fabricate percolating composites using electrically conductive nanoparticles [16, 17]. As the content of the nanoparticles grows to the vicinity of the percolation threshold, these composites exhibit an abrupt increase in dielectric permittivity [1, 18]. It can be several orders of magnitude larger than that of the insulating polymer matrix. This increase is due to an effective increase in the electrode area [19, 20]. When the content of nanoparticles approaches the percolation threshold, the fillers tend to contact each other but still remain insulated by thin polymer layers, forming a large amount of nanocapacitors with conductive nanoparticles as the electrodes and the polymer matrix as dielectrics [19, 21, 22]. Conductive nanoparticles of large aspect ratios can be employed, resulting in lower percolation thresholds relative to traditional composites [23-27]. This could also reduce processing costs and maintain material processability.

Although polymers incorporated with conductive fillers usually showed large enhancement in dielectric permittivity, high loss tangent often arose due to the formation of a conductive network, thus limiting their practical use as dielectric materials for electrical and electronic devices [17, 19, 28]. To obtain a large dielectric permittivity while ensure a low loss tangent, in this study we used copper nanowires (CuNWs) coated with a hydrophobic insulating layer to enhance the dielectric performance of polymer. This as-synthesized insulating layer served for several purposes: (1) protection of CuNWs from being oxidized; (2) attainment of good dispersion of CuNWs in the polymer matrix; (3) prevention of the formation of a conductive network through the resultant composite, thus suppressing the dielectric loss. The resultant polymer nanocomposite displayed high dielectric permittivity, low loss tangent and an appropriate dielectric breakdown strength. Previously, the fabrication and electrical characterization of CuNWs-filled polystyrene (PS) nanocomposites have been well studied [29-35]. Thus in this work PS was used as the matrix material because of its compatibility with the hydrophobic CuNWs. From the literature, high-*k* polymer composites have often been obtained by reinforcing polymers with core-shell spherical nanoparticles [36]. Little information is available on the preparation and properties characterization of high-*k* polymer composites with one-dimensional, core-shell metal nanowires.

2. Experimental

Materials

PS pellets were purchased from Dow Chemical Pacific Ltd. Reagent-grade chemicals copper chloride ($\text{CuCl}_2 \cdot 2\text{H}_2\text{O}$, Sigma-Aldrich, 99 %), octadecylamine (ODA) ($\text{C}_{17}\text{H}_{37}\text{N}$, Sigma-

Aldrich, 90 %), toluene (C_7H_8 , Sigma-Aldrich, 99.7 %), ethanol (C_2H_5OH , Sigma-Aldrich, 99 %) and methanol (CH_3OH , Sigma-Aldrich, 99 %) were used as received without further purification.

Synthesis of CuNWs

In a typical process for synthesizing CuNWs, 2 mM ODA was added to 50 mL of copper chloride (20 mM) aqueous solution and stirred overnight. The formed blue emulsion was transferred into an 80-mL Teflon-lined autoclave and kept at 170 °C for 48 h. By cooling the autoclave to room temperature, the supernatant was decanted and the final product was washed with ethanol, methanol and toluene for three cycles. Finally, the product was suspended in toluene.

Preparation of CuNW/PS nanocomposites

To prepare CuNW/PS nanocomposite films, PS pellets were firstly dissolved in toluene. It was then mixed with different amounts of CuNWs suspension in toluene. The mixed suspensions were then solution cast and dried to give CuNW/PS films with different CuNWs contents. The thickness of the films ranged from 20 to 30 μm . The surface roughness was found to be negligible compared to the film thickness. The films were then fractured in liquid nitrogen for their morphological observations.

Characterization

CuNWs were examined in a transmission electron microscope (TEM; Philips FEG CM 20). X-ray diffraction (XRD) patterns of these nanowires were recorded with a Bruker D2 Phaser

(Cu tube with $\lambda = 1.54184 \text{ \AA}$). Fourier transform infrared (FTIR) spectra were recorded on a Perkin Elmer precisely Spectrum 100 spectrometer. The morphology of CuNWs and the CuNW/PS composites were observed in a scanning electron microscope (SEM; Jeol JSM 820) and field emission scanning electron microscope (FESEM; FEG JSM 6335). The dielectric performance of these composites was measured with an Agilent 4284A Precision LCR Meter. The AC voltage applied was 200 mV. The dielectric permittivity of the composites showed a very weak dependence on the AC voltage. Highly conductive silver ink was coated on the specimen surfaces to form electrodes, and their inductance was neglected. The breakdown strength of the samples was measured in silicon oil at room temperature with a Trek Model 609E-6-FG high voltage amplifier under a ramp rate of 200 V/s. The samples were cut to sizes of 25 cm^2 .

3. Results and Discussion

ODA served as both a reducing agent and a capping agent in the reaction system. It has been well known that long-chain primary amines are mild reducing agent for metal ions [37]. Although ODA is difficult to be dissolved in water, it can almost be totally dissolved in the aqueous solution of copper chloride. The presence of lone pair of electrons on the nitrogen atom of ODA renders it both basic and nucleophilic. As such, ODA molecules would coordinate with Cu^{2+} in aqueous solution. X-ray Diffraction (XRD) of the corresponding cast film from the dispersion exhibits periodic peaks (Figure 1), demonstrating a well-ordered structure. The long spacing (4.15 nm) of the aggregates obtained from the XRD experiments is slightly smaller than twice the evaluated monomolecular length of ODA obtained from the CPK model (2.42 nm), but

it is much larger than the monomolecular length, indicating that ODA assembles into bilayer membranes bearing a slightly interdigitation packing model in the CuCl_2 solution (Scheme 1).

Israelachvili and co-workers proposed the packing parameter concept, i.e. formation of the micelles for single-chain surfactants, and bilayers for double-chain surfactants [38]. In the ODA- CuCl_2 dispersion, a Cu^{2+} coordinates with two ODA molecules to form pseudo-double-tailed surfactants with a coordinated headgroup, and then self-assemble into bilayers, causing the dissolution of ODA in CuCl_2 solution. In a previous work, Luo et al. reported that ODA also coordinated with Ag^+ to form a double-chain surfactant that assembled into bilayers in water [39].

The strong interaction of ODA to Cu^{2+} facilitates electron transfer between them. Under hydrothermal conditions the coordinated electrons were captured by Cu^{2+} , causing a continuous formation of zero-valence copper atoms, which in turn come together to form nuclei (Scheme 2A). Due to the binding of protonized ODA on these nuclei, they would not aggregate into large particles. The subsequent growth of these nuclei resulted in a distribution of multiply twinned, singly twinned, and single-crystal seeds, with the 5-fold twinned decahedron being the lowest in free energy and thus the most abundant morphology (Scheme 2B) [40]. Consequently, protonized ODA molecules play the role of capping agent such that they adhere to the (100) faces of the seeds (Scheme 2C) and inhibit the growth of these faces, thus direct the growth of these seeds into nanowires (Scheme 2D). A more detailed study of the growth of CuNWs will be given elsewhere.

The synthesized CuNWs can be easily dispersed in nonpolar solvents such as toluene (Figure 2A) and hexane, but are poorly dispersed in water, indicating their hydrophobic nature. Low magnification SEM image shows that the nanowires are 40-150 nm in diameter, and they have remarkable lengths up to several hundred micrometers (Figure 2B). The nanowires tend to self-assemble into bundles, as Figure 2C shows. The diameter of the bundles ranges from several hundred nanometers up to several micrometers. The molar ratio of ODA to CuCl_2 is found to play an important role in regulating the morphologies of the products. Excessive ODA would limit the radial growth of the nanowires to a greater degree, thus is helpful for the synthesis of thinner nanowires (Figure 2C and 2D). Too much ODA, however, would cap the growing facets of copper nanocrystals and cause the formation of copper nanoparticles (Figure 2D).

The TEM micrographs (Figure 3) show that the CuNWs are highly flexible and are coated with a thin organic layer. As mentioned above, the binding of protonized ODA to CuNWs resulted in this layer. Due to the hydrophobic nature of this layer, it would trigger hydrophobic-hydrophobic interactions among the nanowires and produce nanowire bundles as shown in Figure 2C [41]. The thickness of the layers ranged from 2 to 8 nm, and it could not be easily removed after several washing cycles, indicating their strong adherence to the CuNWs.

The insulating layer on the CuNWs can be detected by XRD, as shown in Figure 4. The weak diffraction of CuNWs at 22.5° corresponds to the ODA peak at about 21° , implying an additional phase of ODA derivatives. The diffraction peaks of CuNWs at 43.2° , 50.4° and 74.1° correspond to the (111), (200) and (220) planes of Cu, respectively. The oxides of copper, such

as Cu_2O and CuO , are not observed, implying this layer is dense and tightly bind to the CuNWs, thus preventing the permeation of oxygen to the copper core.

FTIR spectra obtained from the ODA, cast ODA- CuCl_2 film and synthesized CuNWs in the range $2500\text{--}3500\text{ cm}^{-1}$ are shown in Figure 5. The spectra shows that a prominent feature occurs at 3335 cm^{-1} in ODA, corresponding to the N-H stretch vibrations from uncoordinated ODA molecules. This feature is completely lost in the ODA- CuCl_2 film (curve B), implying that all ODA molecules are coordinated to Cu^{2+} ions (curve B). This coordination yields three additional modes at 3268 cm^{-1} , 3240 cm^{-1} and 3257 cm^{-1} (curve B). Such a shift in the N-H stretch vibration mode on the formation of salts with anions, such as PtCl_6^- , has been observed in Langmuir–Blodgett films of ODA [42], and ODA-stabilized colloidal gold nanoparticles [43]. For CuNWs, the N-H vibrational feature is indiscernible, due to the removal of most ODA derivatives by the washing process. Nonetheless, the methylene anti-symmetric and symmetric vibrations are still observed at 2918 and 2851 cm^{-1} (curve C), respectively, substantiating the existence of alkyl chains on the CuNWs. The alkyl chains bond to the nanowires via the $-\text{NH}_2^+$ head group, as in the case of the adsorption of cetyltrimethylammonium headgroup to gold nanorod surfaces [44-46].

The hydrophobic nature of the CuNWs makes them compatible with nonpolar PS. Figure 6 shows the SEM micrographs of CuNW/PS nanocomposites at different CuNWs contents. The porosity in Figure 6 was caused by the pull-out of CuNWs from the PS matrix during SEM sample preparation. No agglomeration of CuNWs within the composite was observed. The

hydrophobic coating layer on the CuNWs enabled them to interact strongly with nonpolar PS molecular chains, causing the nanowires to be effectively disentangled and dispersed. Due to the interaction of PS with them, CuNWs would orient randomly during the solution casting process. It is noted that ODA has also been used to modify other conductive filler materials, such as graphene [47-49], to make it hydrophobic and dispersible in a variety of nonpolar solvents. Figure 7 shows that the PS tended to crystallize on the nanowires and most CuNWs were located at the center of the PS spherulites.

The ability of a dielectric material to store energy is mainly related to the polarization of the material, i.e. electric field-induced electric moment in the material, which result in an increase in capacitance. In a dielectric material, four kinds of polarization exist: electronic, atomic, orientational and interfacial polarizations. At lower frequencies all the four types of polarization may contribute but as the frequency increases the orientation and space charge contribution decreases. Hence the relative permittivity gradually decreases as a function of frequency. Polar polymers have permanent dipole moments, thus they generally have a larger dielectric permittivity than nonpolar polymers. For instance, polar polyvinylidene fluoride has a larger dielectric permittivity ($\epsilon' = 8$) than nonpolar PS ($\epsilon' = 2.5$). At higher frequency, orientation polarization decreases and the electronic and atomic polarizations predominate. For a heterogeneous composite material with different conductivity/dielectric permittivity (σ/ϵ') ratio between the matrix and the filler material, interfacial polarization (Maxwell-Wagner-Sillars polarization), also contributes to the dielectric permittivity. The interfacial polarization is caused by the discontinuity of the material and generated by the accumulation of charges at the

interfaces. It generally occurs at about the same frequency range as orientation polarization. Thus it can be regarded as a large dipole polarization, in which the electric dipole is related to the strength of each charge and the separation between charges. Nanocomposite material generally has a large interfacial region due to the huge surface area of nanofillers. This enables it to accommodate large amount of charges when exposed to an alternate electric field, resulting in a pronounced interfacial polarization.

Figure 8A shows that the dielectric permittivity of CuNW/PS nanocomposite rises significantly with increasing CuNWs content. At a 16 wt.% CuNWs loading, the dielectric permittivity of the composite reaches 37 at 1 MHz, which is about 14 times larger than that of pure PS. In a classic percolation model [50, 51], the randomly distributed conductive fillers form clusters (conducting networks) within the insulating matrix. When the size of the largest cluster approaches a critical value, discharge between the electrodes (percolation) happens. The percolation model predicts that the variation of dielectric permittivity with filler content follows a power law relation [52]

$$\varepsilon' = A|p_c - p|^q \quad (1)$$

where p_c , p and q are the percolation threshold, CuNWs volume fraction and a critical exponent; and A is a constant. As shown in Figure 8B, the increase of dielectric permittivity shows a good agreement with Equation 1, indicating that although the CuNWs had a core-shell structure, the dielectric permittivity of the resultant CuNW/PS nanocomposites can still be described by the percolation model.

Since PS is nonpolar, its dielectric properties show intrinsic weak frequency dependent behavior. By incorporating CuNWs up to 12 wt.%, a stable dielectric permittivity over a wide range of frequency is still observed (Figure 8A). The dielectric permittivity shows weak frequency dependency as the CuNWs content increases to 16 wt.%, implying that the interfacial polarization becomes more predominant at high CuNWs loading. Because the relaxation time of interfacial polarization is reversely proportional to the electrical conductivity of the fillers [53], the high conductivity of copper ($\sim 6 \times 10^5$ S/cm) is expected to drastically reduce the relaxation time, allowing the interfacial polarization to be able to respond quickly to the alternating electric field. This indicates that at higher frequency range, where electric field alternates very fast, the charges are still capable of piling up swiftly at the interfacial region, contributing to dielectric permittivity.

Figure 8C shows the dielectric loss of the CuNW/PS nanocomposites. It can be observed that the dielectric loss rises significantly with CuNWs content. This is attributed to enhanced polarization and Ohmic losses. The magnified polarization loss arising from interfacial polarization is a significant factor in producing high dielectric loss at higher filler contents. The decaying trend of dielectric loss with frequency can be ascribed to reduced polarization losses at high frequency. Due to interfacial polarization relaxation, the interfacial charge polarization becomes weaker at high frequency, resulting in lower polarization loss. Moreover, an increase in CuNWs content would reduce the average distance between the nanowires. This would increase the chance of the electrons to tunnel and/or hop between adjacent nanowires in each half cycle of

alternating field, thereby leading to conduction loss. Due to the insulating coating layer on the CuNWs, it is proposed that the polarization loss plays a more dominant role.

Both electric dipoles and interfacial polarization try to follow the direction of electric field. The required adjustment period corresponds to the relaxation time of them. The faster the electric field alternates, the longer the orientation lags behind the field and the greater is the electrical energy consumed. Available power output thus decreases because electric power is partly lost by converting into thermal energy. The extent to which the energy is dissipated can be characterized by the dielectric loss tangent ($\tan\delta$). The lower the loss tangent of a dielectric material, the better is its performance for charge storage applications. Mathematically, $\tan\delta$ can be expressed as the ratio of imaginary dielectric permittivity ϵ'' to real dielectric permittivity ϵ' :

$$\tan\delta = \epsilon''/\epsilon'.$$

The loss tangent of an insulating material is of great technological importance, because it quantifies the fraction of energy dissipated in a capacitor. From Figure 9, the loss tangent of CuNW/PS nanocomposites displays a frequency-dependent behavior. The decaying trend of loss tangent with frequency is a manifestation that interfacial polarization grows weaker at higher frequency. Besides, although the loss tangent of CuNW/PS nanocomposites increases with filler content, it maintains at a relatively low level (< 0.04 at 1 MHz) (Figure 9). The conduction loss mentioned before is linked to the dissipation of energy in phase with an alternating field, and contributes an additional $\sigma/2\pi f\epsilon'$ to the loss tangent of the material. Since frequency increase is equivalent to reduced available times for free electrons to travel between the CuNWs in each half cycle of alternating field, it would therefore reduce the conduction loss.

The lower loss tangent of the CuNW/PS nanocomposites is ascribed to the presence of an insulating coating layer on the surface of CuNWs, which impairs the formation of a conductive network at higher CuNWs contents, thus drastically suppressing the conduction loss ($\sigma/2\pi f\epsilon'$). Figure 10A shows the dependency of the 40 Hz conductivity of CuNW/PS composites on the CuNWs content; the linear dependency of conductivity on frequency as shown in Figure 10B reveals their insulating nature. Therefore, hydrophobic coating layer on the CuNWs cuts the available free path of the nomadic charges and reduces the otherwise possible leaky current. The increase in conductivity with CuNWs contents is due to the increased dissipating charge carriers. As mentioned before, their hopping or tunneling would contribute to the electrical conduction.

The dielectric breakdown strength (E_B) of an insulating material is closely related to its ability to store electrical energy. Figure 11 gives the dielectric breakdown strength of CuNW/PS nanocomposite with different nanowire contents. Apparently, the breakdown field strength gradually decreases with the increase in CuNWs content, as expected. The maximum energy density (U_M) is related to the breakdown strength by the expression: $U_M = \epsilon_0\epsilon'E_B^2/2$ ($\epsilon_0 = 8.85 \times 10^{-12}$ F/m). Figure 11 shows that U_M is rather low (< 1 J/cm³) at low filler contents (≤ 12 wt.%), due to the small dielectric permittivity of the material. The drastic increase in U_M at 16 wt.% content is caused by the large dielectric permittivity (Figure 8A) and the acceptable low level of E_B . An energy density as high as 2 J/cm³ is obtained at a field strength of 300 V/ μ m.

4. Conclusions

In summary, we have presented the synthesis of hydrophobic CuNWs with a core-shell structure and the use of them to improve the dielectric performance of PS. It is demonstrated that the obtained CuNW/PS nanocomposites exhibit large improvement in dielectric permittivity and a relatively low loss tangent. The large dielectric permittivity was caused by the strong interfacial polarization. The low loss tangent was due to the hydrophobic insulating layer on the CuNWs, which averted the direct contact between the nanowires and maintained insulating nature of the resultant composite material. Our method can be potentially used to develop high-k nonpolar polymer nanocomposites for electrical applications.

Acknowledgment

This work is supported by the project (R-IND4401), Shenzhen Research Institute, City University of Hong Kong.

References

- [1] Z. M. Dang, J. K. Yuan, J. W. Zha, T. Z. Zhou, S. T. Li and G. H. Hu, *Prog. Mater. Sci.*, 2012, **57**, 660-723.
- [2] R. Popielarz, C. K. Chiang, R. Nozaki and J. Obrzut, *Macromolecules*, 2001, **34**, 5910-5915.
- [3] P. Barber, S. Balasubramanian, Y. Anguchamy, S. Gong, A. Wibowo, H. Gao, H. J. Ploehn and H. C. Zur Loye, *Materials*, 2009, **2**, 1697-1733.
- [4] S. C. Tjong and G. D. Liang, *Mater. Chem. Phys.*, 2006, **100**, 1-5.
- [5] S. C. Tjong and Y. Z. Meng, *Eur. Polym. J.*, 2000, **36**, 123-129.

- [6] X. H. Li, S. C. Tjong, Y. Z. Meng and Q. Zhu, *J. Polym. Sci. Part B: Polym. Phys.*, 2003, **41**, 1806-1813.
- [7] K. L. Fung, R. K. Y. Li and S. C. Tjong, *J. Appl. Polym. Sci.*, 2002, **85**, 169-176.
- [8] L. He and S. C. Tjong, *Current Nanosci.*, 2010, **6**, 40-44.
- [9] Y. Rao, S. Ogitani, P. Kohl and C. P. Wong, *J. Appl. Polym. Sci.*, 2002, **83**, 1084–1090.
- [10] S. Thomas, V. Deepu, S. Uma, P. Mohanan, J. Philip and M. T. Sebastian, *Materials Science and Engineering B*, 2009, **163**, 67–75.
- [11] G. Subodh, V. Deepu, P. Mohanan and M. T. Sebastian, *Polym. Eng. Sci.*, 2009, **49**, 1218-1224.
- [12] S. George, V. Deepu, P. Mohanan and M. T. Sebastian, *Polym. Eng. Sci.*, 2010, **50**, 570-576.
- [13] S. George, P. S. Anjana, M. T. Sebastian, J. Krupka, S. Uma and J. Philip, *Int. J. Appl. Ceram. Technol.*, 2010, **7**, 461–474.
- [14] S. George and M. T. Sebastian, *Compos. Sci. Tech.*, 2009, **69**, 1298–1302.
- [15] A. S. Bhalla, R. E. Newnham, L. E. Cross, W. A. Schulze, J. P. Dougherty and W. A. Smith, *Ferroelectrics* 1981, **33**, 139-146.
- [16] K. S. Deepa, M. T. Sebastian and J. James, *Appl. Phys. Lett.*, 2007, **91**, 202904.
- [17] K. S. Deepa, S. Kumari Nisha, P. Parameswaran, M. T. Sebastian and J. James, *Appl. Phys. Lett.*, 2009, **94**, 142902.
- [18] S. Wageh, L. He, A. A. Al-Ghamdi, Y. A. Al-Turki and S. C. Tjong, *RSC Adv.*, 2014, **4**, 28426-28431.
- [19] M. J. Jiang, Z. M. Dang, M. Bozlar, F. Miomandre and J. B. Bai, *J. Appl. Phys.*, 2009, **106**, 084902.

- [20] B. E. Kilbride, J. N. Coleman, J. Fraysse, P. Fournet, M. Cadek, A. Drury, S. Hutzler, S. Roth and W. J. Blau, *Appl. Phys. Lett.*, 2002, **92**, 4024-4030.
- [21] M. Arjmand, T. Apperley, M. Okoniewski, U. Sundararaj and S. Park, *Carbon*, 2012, **50**, 5126-5134.
- [22] G. D. Liang, S. P. Bao and S. C. Tjong, *Mater. Sci. Eng. B*, 2007, **142**, 55-61.
- [23] L. He and S. C. Tjong, *RSC Adv.*, 2013, **3**, 22981-22987.
- [24] L. He and S. C. Tjong, *Nanoscale Res. Lett.*, 2013, **8**, 132.
- [25] L. He and S. C. Tjong, *J. Nanosci. & Nanotech.*, 2011, **11**, 10668-10672.
- [26] L. He and S. C. Tjong, *J. Nanosci. & Nanotech.*, 2011, **11**, 3916-3921.
- [27] L. He and S. C. Tjong, *Current Nanosci.*, 2010, **6**, 520-524.
- [28] Y. C. Li, S. C. Tjong and R. K. Y. Li, *Synth. Met.*, 2010, **160**, 1912-1919.
- [29] B. Lin, G. A. Gelves, J. A. Haber and U. Sundararaj, *Ind. Eng. Chem. Res.*, 2007, **46**, 2481-2487.
- [30] B. Lin, G. A. Gelves, J. A. Haber, P. Pötschke and U. Sundararaj, *Macromol. Mater. Eng.*, 2008, **293**, 631-640.
- [31] G. A. Gelves, B. Lin, J. A. Haber and U. Sundararaj, *J. Polym. Sci.: Part B: Polym. Phys.*, 2008, **46**, 2064-2078.
- [32] G. A. Gelves, M. H. Al-Saleh and U. Sundararaj, *J. Mater. Chem.*, 2011, **21**, 829-836.
- [33] G. A. Gelves, B. Lin, U. Sundararaj and J. A. Haber, *Nanotechnology*, 2008, **19**, 215712.
- [34] M. H. Al-Saleh, G. A. Gelves and U. Sundararaj, *Composites: Part A*, 2011, **42**, 92-97.
- [35] C. Schmädicke, M. Poetschke, L. D. Renner, L. Baraban, M. Bobeth and G. Cuniberti, *RSC Adv.*, 2014, **4**, 46363-46368.

- [36] X. Huang and P. Jiang, *Adv. Mater.*, 2015, **27**, 546-554.
- [37] D. S. Wang and Y. D. Li, *Inorg. Chem.*, 2011, **50**, 5196-5202.
- [38] J. N. Israelachvili, D. J. Mitchell and B. W. Ninham, *J. Chem. Soc., Faraday Trans.*, 1976, **2**, 1525-1568.
- [39] X. Luo, W. Miao, S. Wu and Y. Liang, *Langmuir*, 2002, **18**, 9611-9612.
- [40] L. D. Marks, *Rep. Prog. Phys.*, 1994, **57**, 603-649.
- [41] E. Y. Ye, S. Y. Zhang, S. H. Liu and M. Y. Han, *Chem. Euro. J.*, 2011, **17**, 3074-3077.
- [42] M. Bardosova, R. H. Tredgold and Z. Ali-Adib, *Langmuir*, 1995, **11**, 1273-1276.
- [43] S. Murali, K. Ashavani and M. Priyabrata, *Colloids and Surfaces A: Physicochemical and Engineering Aspects*, 2001, **181**, 255-259.
- [44] C. J. Murphy, T. K. Sau, A. Gole and C. J. Orendorff, *MRS Bulletin*, 2005, **30**, 349-355.
- [45] J. Gao, C. M. Bender and C. J. Murphy, *Langmuir*, 2003, **19**, 9065-9070.
- [46] C. J. Murphy, T. K. Sau, A. Gole, C. J. Orendorff, J. Gao, L. Gou, S. Hunyadi and T. Li, *J. Phys. Chem. B*, 2005, **109**, 13857-13870.
- [47] S. Niyogi, E. Bekyarova, M. E. Itkis, J. L. McWilliams, M. A. Hamon and R. C. Haddon, *J. Am. Chem. Soc.*, 2006, **128**, 7720-7721.
- [48] Y. Cao, J. Feng and P. Wu, *Carbon*, 2010, **48**, 1683-1685.
- [49] Y. S. Yun, Y. H. Bae, D. H. Kim, J. Y. Lee, I.-J. Chin and H. J. Jin, *Carbon*, 2011, **49**, 3553-3559.
- [50] S. Kirkpatrick, *Rev. Mod. Phys.*, 1973, **45**, 574-588.
- [51] C. W. Nan, *Prog. Mater. Sci.*, 1993, **37**, 1-116.
- [52] D. R. Bowman and D. Stroud, *Phys. Rev. B*, 1989, **40**, 4641-4650.

[53] T. Blythe and D. Bloor. *Electrical Properties of Polymers*. 2nd Edit, Cambridge University Press, 2005.

Figure captions:

Figure 1 Small angle XRD pattern of cast ODA-CuCl₂ film indicating the strong interaction between ODA and Cu²⁺.

Figure 2 A) Stable dispersion of CuNWs in toluene stabilized by PS (10 mg/ml). B) SEM micrograph of as synthesized CuNWs. C) SEM micrograph of two CuNW bundles. Inset: A very thick CuNW bundle with a diameter of 5 μm. D) SEM micrograph of the mixture of CuNWs, Cu nanoparticles and remnant ODA and/or its derivatives.

Figure 3 TEM micrographs of CuNWs at A) low and B) high magnifications showing the presence of a surface coating layer.

Figure 4 XRD patterns of ODA and the as-synthesized CuNWs.

Figure 5 FTIR spectra of A) ODA, B) cast ODA-CuCl₂ film and C) CuNWs.

Figure 6 SEM micrographs of CuNW/PS nanocomposite at different filler weight fractions. A): 2 wt.%; B): 5 wt.%; C) and D): 8 wt.%;

Figure 7 SEM micrographs of CuNW/PS nanocomposite showing the crystallization of PS on CuNWs.

Figure 8 A) Frequency dependency of real dielectric permittivity of CuNW/PS nanocomposites. B) The best fit of the 1 kHz ϵ' data to Equation 1. The density of the core-shell CuNWs was evaluated to be about 5 g/cm³. C) Frequency dependency of imaginary dielectric permittivity of CuNW/PS nanocomposites.

Figure 9 Frequency dependency of loss tangent of CuNW/PS nanocomposite with different filler contents. The inset shows the loss tangent of CuNW/PS nanocomposites at 1 MHz.

Figure 10 A) The 40 Hz conductivity and B) AC conductivity of CuNW/PS nanocomposites at different filler contents.

Figure 11 Breakdown field strength and maximum energy density of CuNW/PS nanocomposites at room temperature with different filler contents.

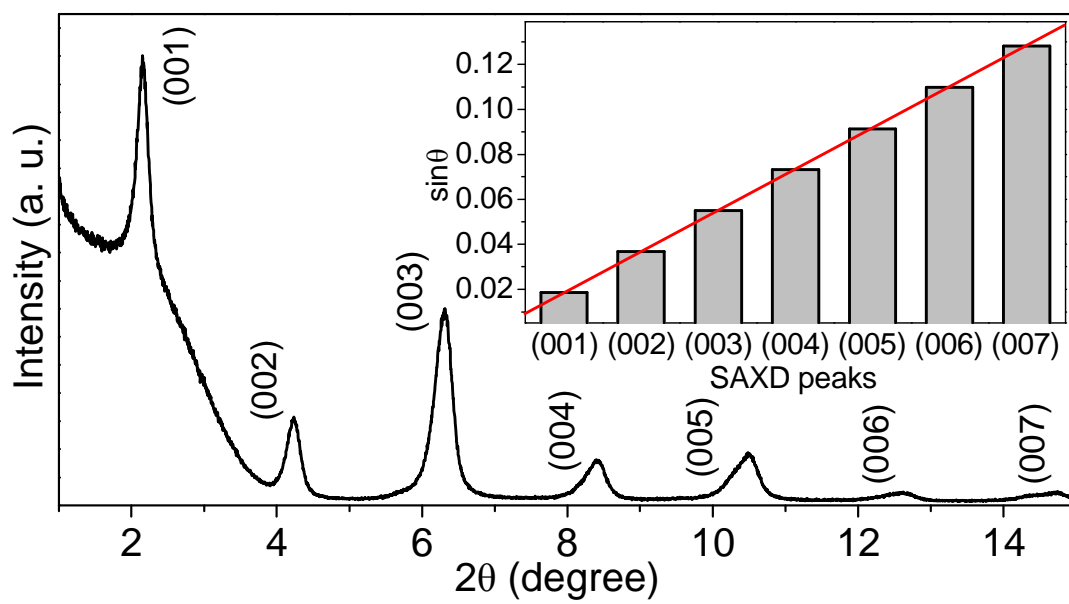


Figure 1

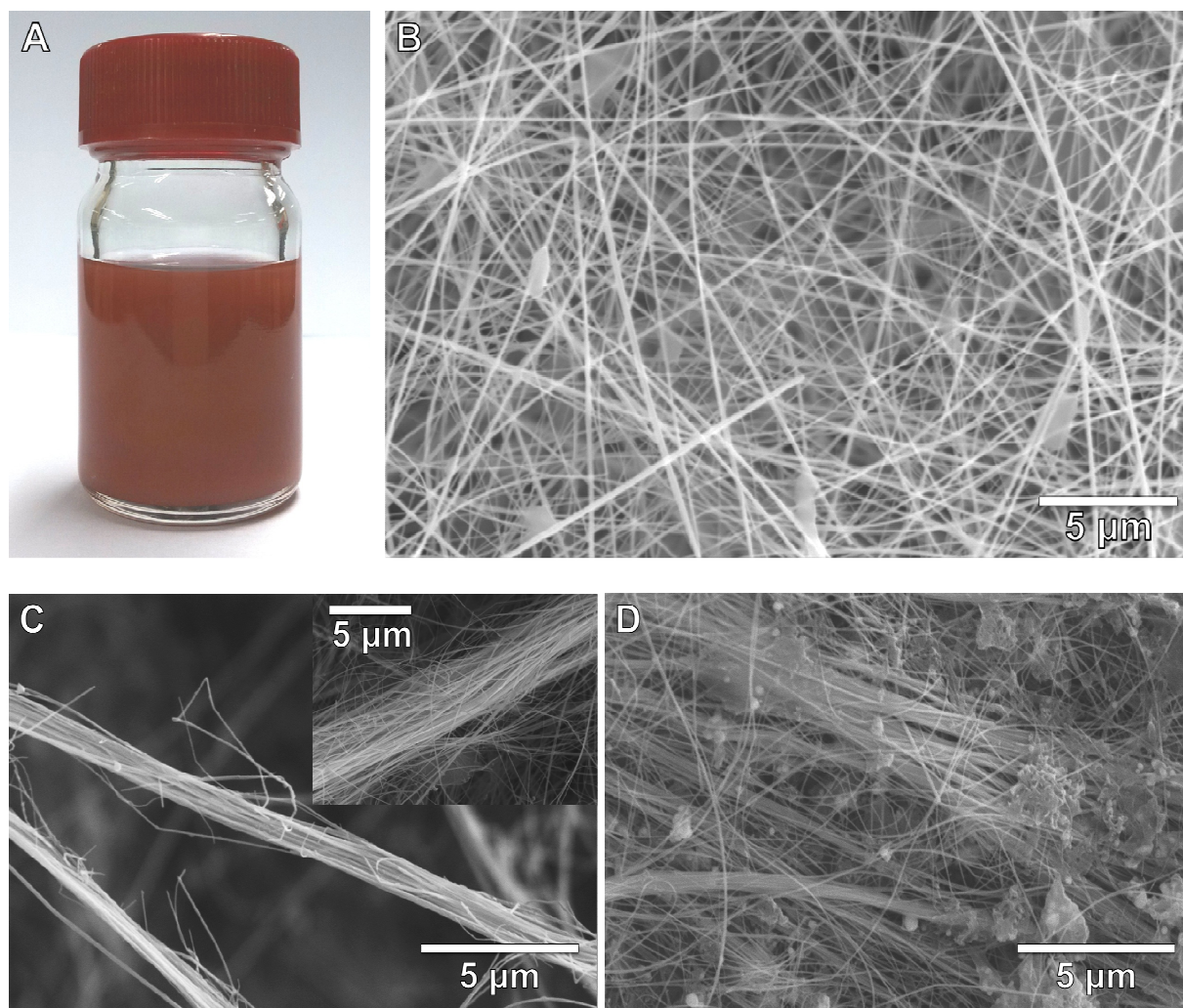


Figure 2

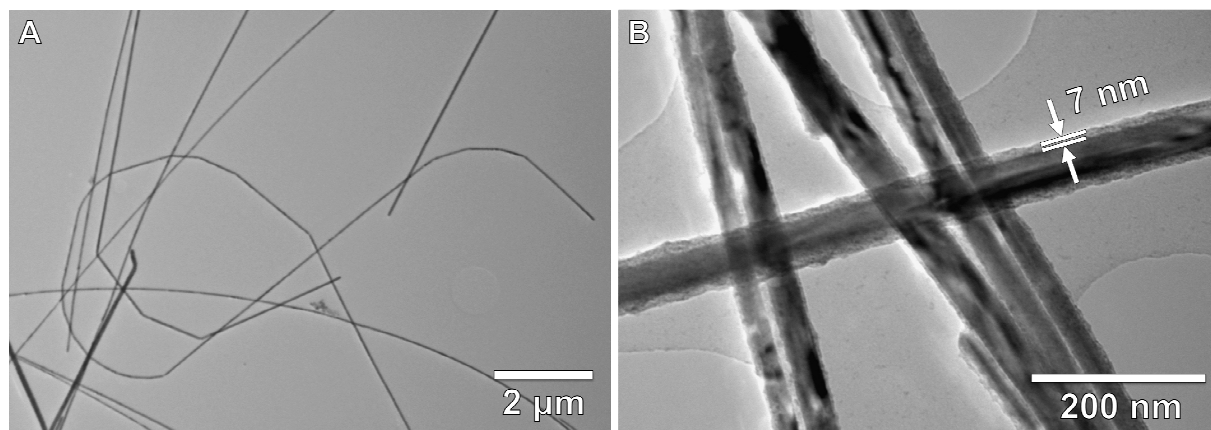


Figure 3

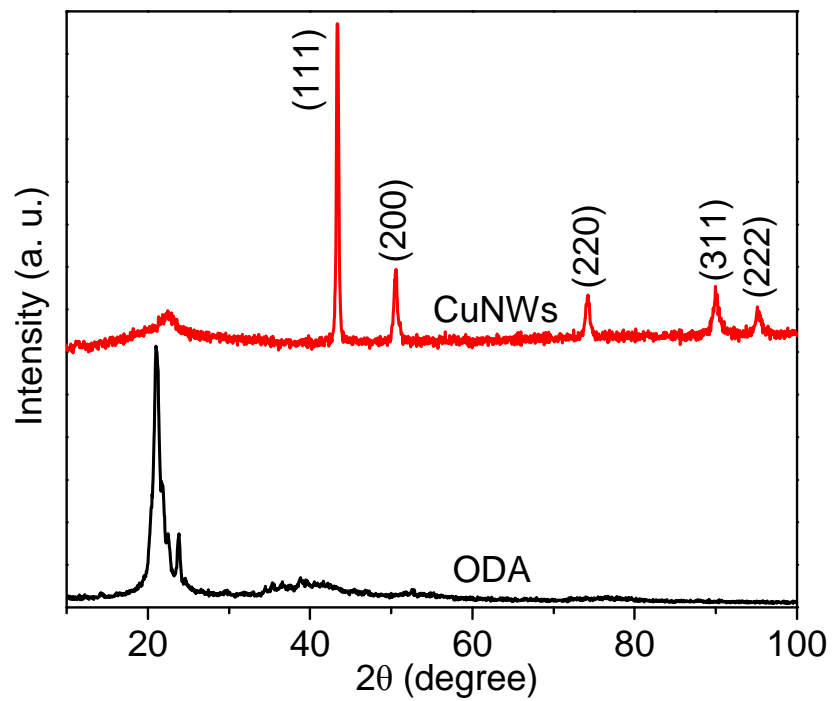


Figure 4

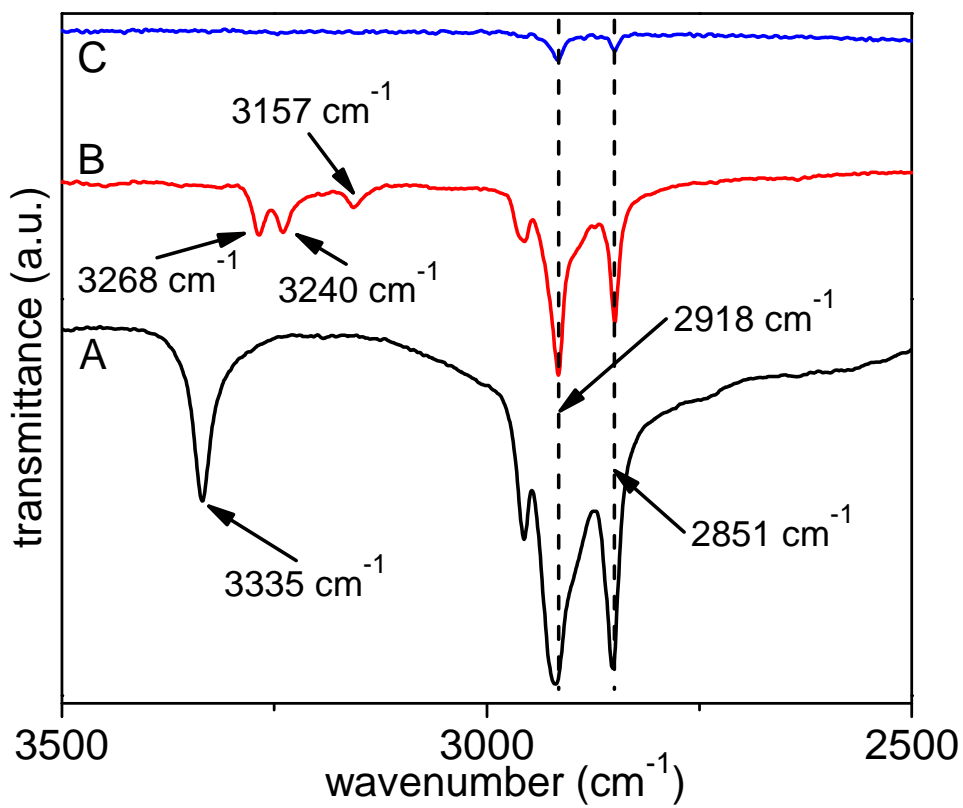


Figure 5

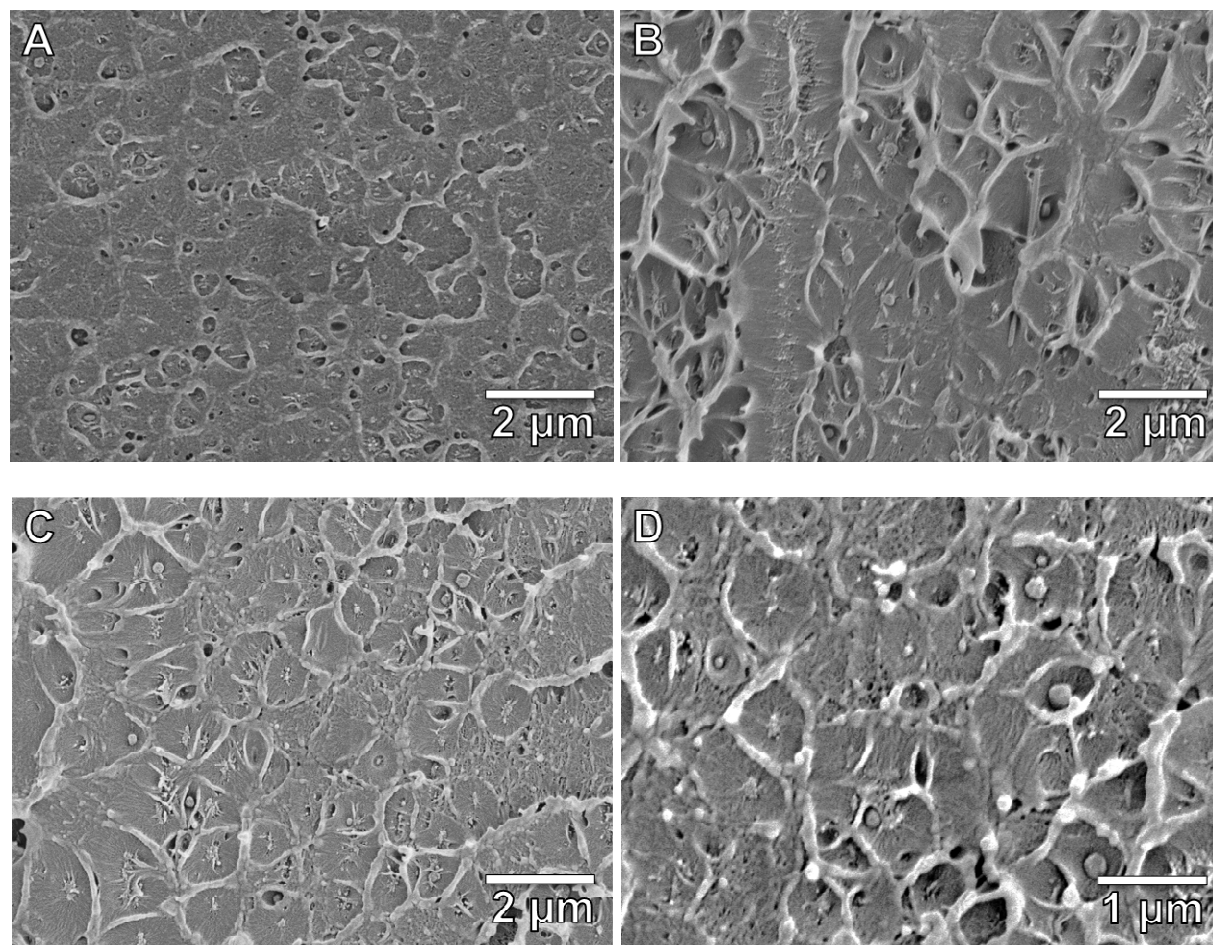


Figure 6

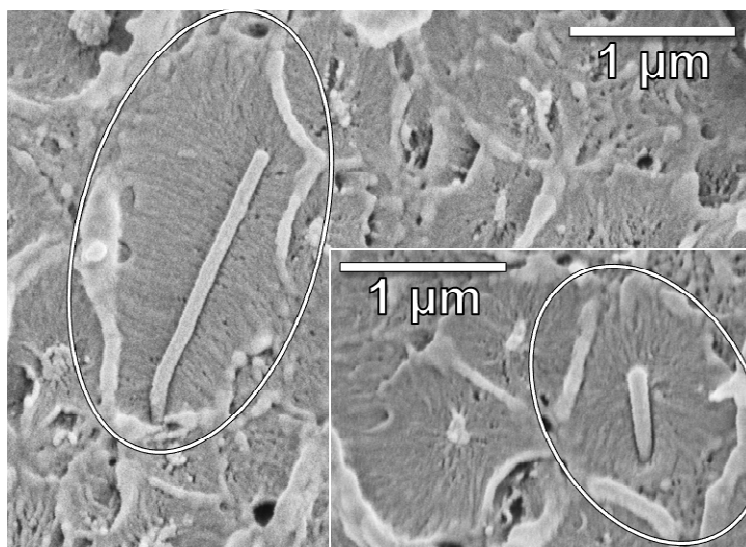
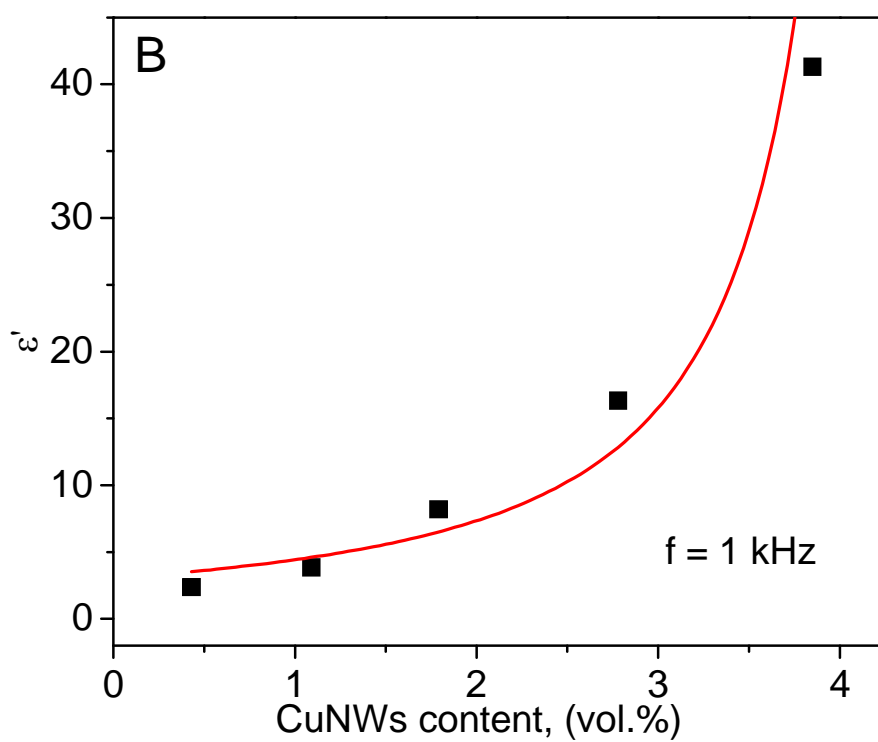
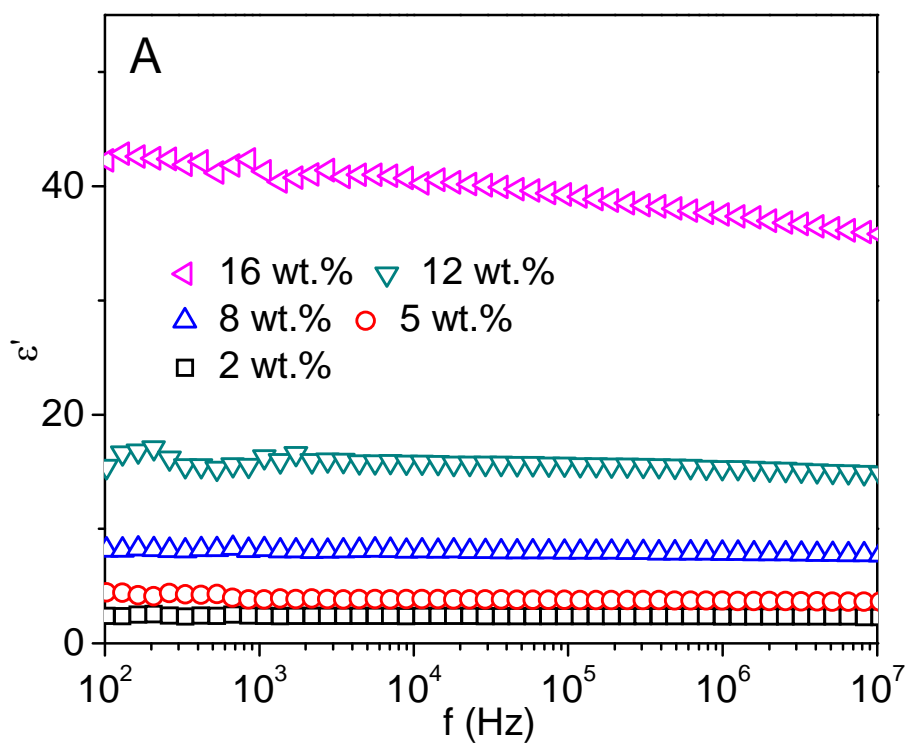


Figure 7



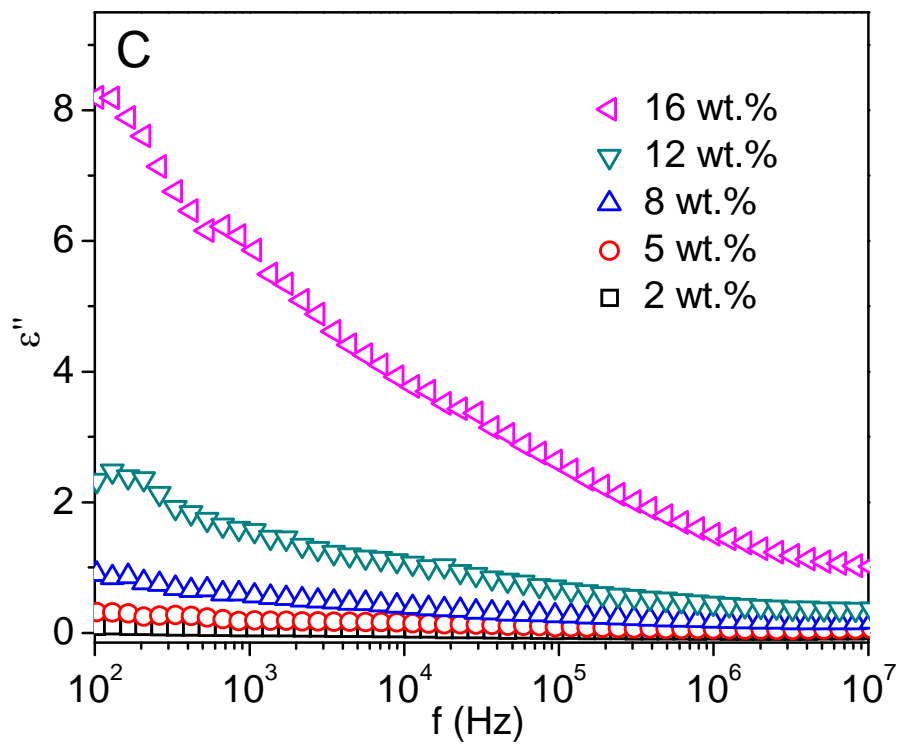


Figure 8

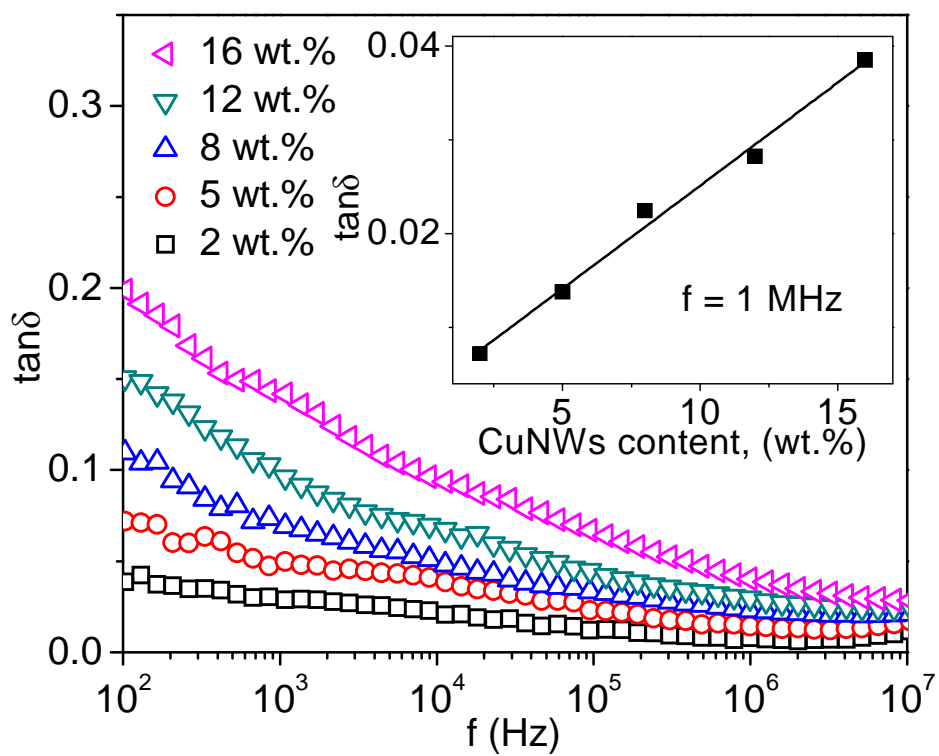


Figure 9

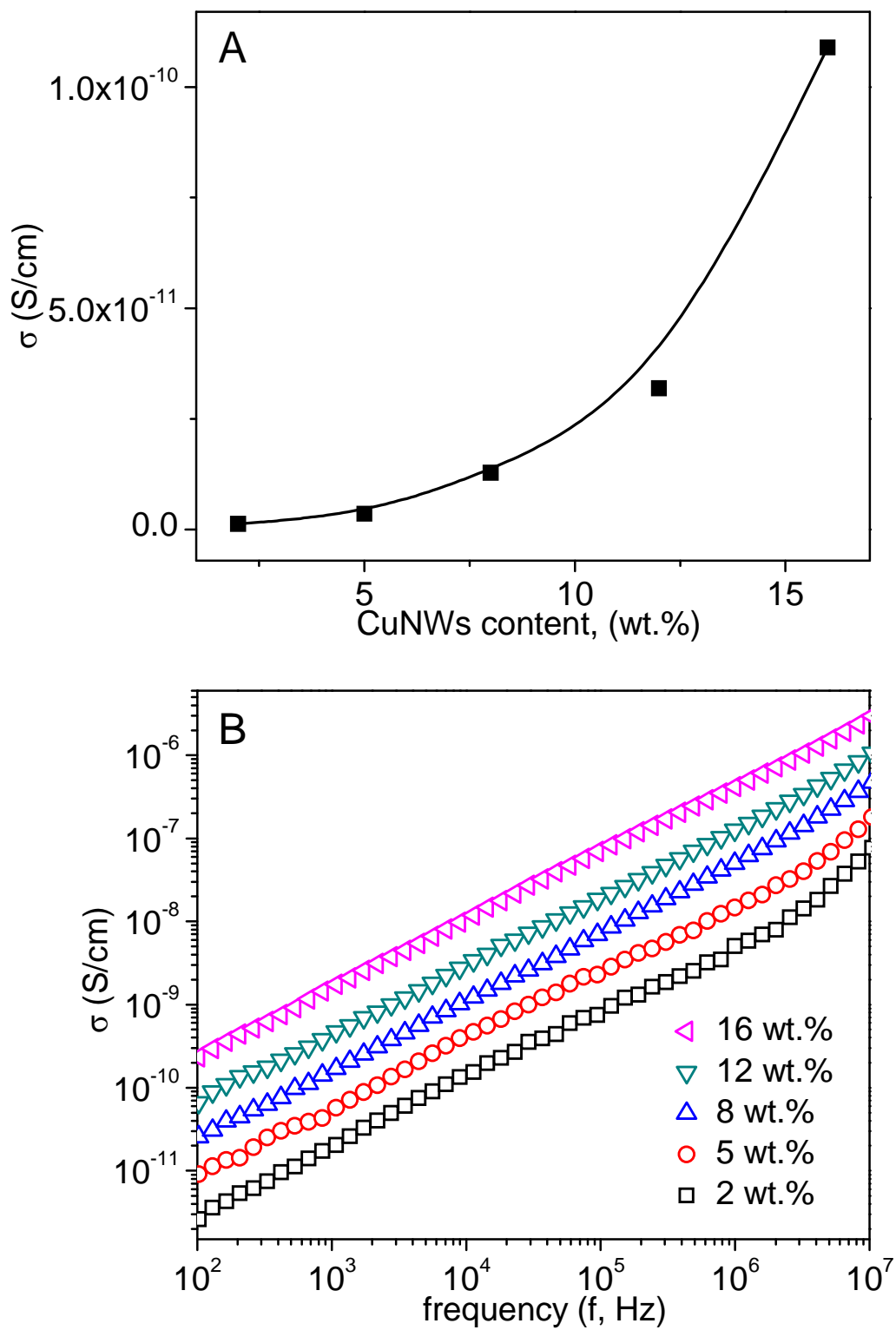


Figure 10

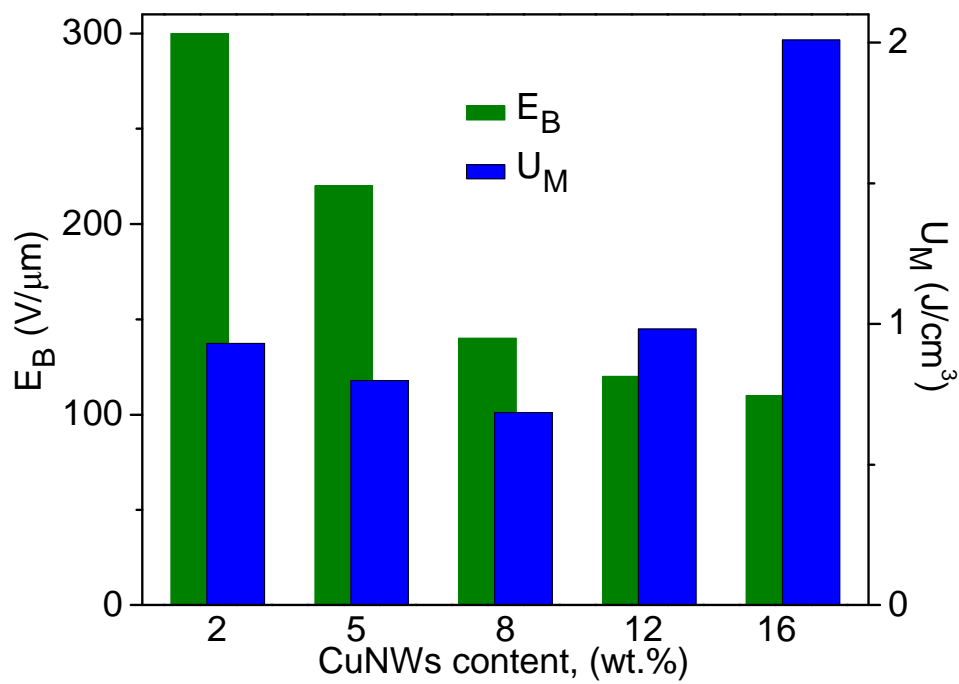
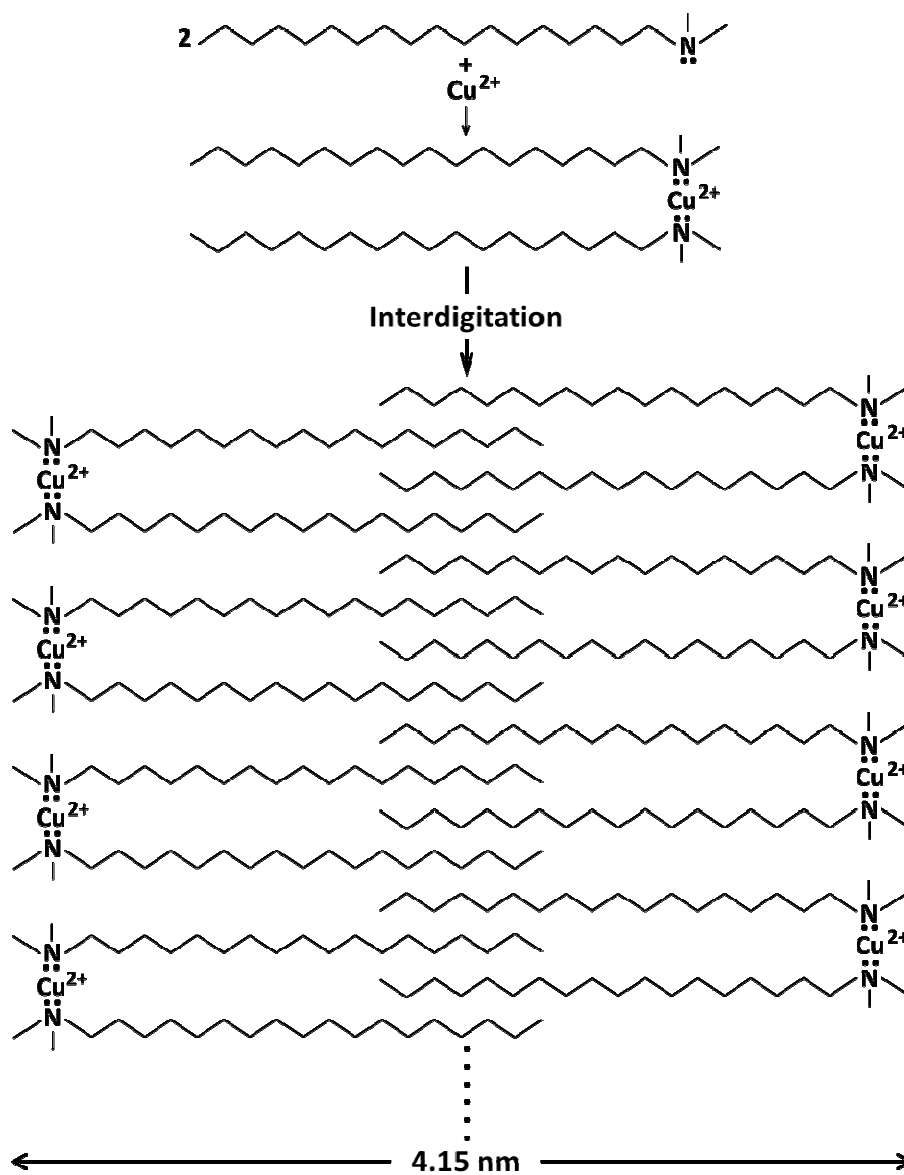


Figure 11

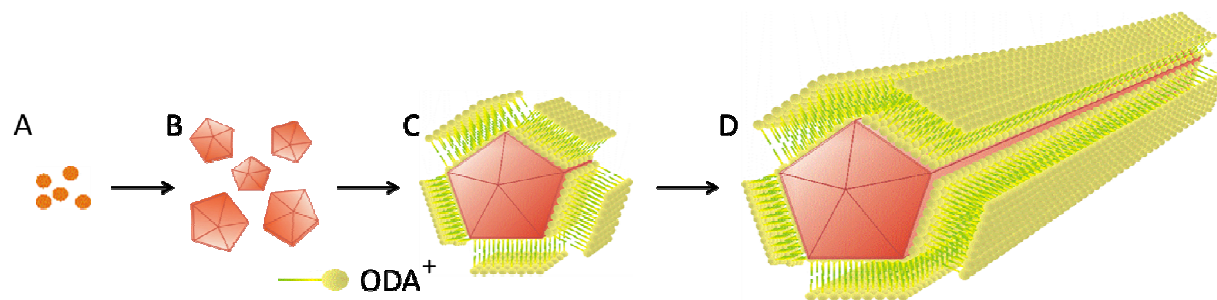
Schemes

Scheme 1 Coordination of ODA to Cu^{2+} to form $\text{Cu}(\text{ODA})_2^{2+}$, which acted as a pseudo-double-tailed cationic surfactant and assembled into bilayers through interdigitation, causing the dissolution of ODA in water.

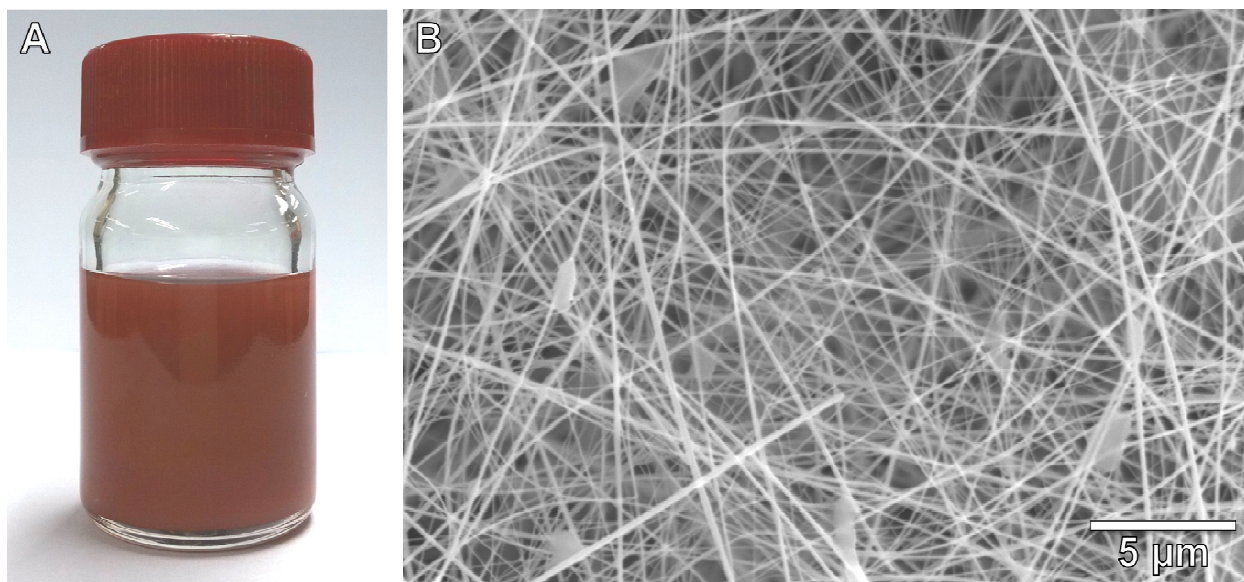
Scheme 2 Growth process of CuNWs. A) Nucleation of copper seeds; B) Growth of copper seeds into 5-fold twinned decahedron; C) Selective capping of the newly developed (100) facets by ODA^+ bilayers; D) Directed growth of a copper seed into a nanowire.



Scheme 1



Scheme 2



Core-shell copper nanowires for improving the dielectric performance of polystyrene